

# Low-noise on-chip frequency conversion by four-wave-mixing Bragg scattering in $\text{SiN}_x$ waveguides

Imad Agha,<sup>1,2,†,\*</sup> Marcelo Davanço,<sup>1,2,†</sup> Bryce Thurston,<sup>1</sup> and Kartik Srinivasan<sup>1,\*</sup>

<sup>1</sup>Center for Nanoscale Science and Technology, National Institute of Standards and Technology, Gaithersburg, MD 20899

<sup>2</sup>Maryland NanoCenter, University of Maryland, College Park, MD 20742

<sup>†</sup>These authors contributed equally. \* e-mail: imad.gha@nist.gov; kartik.srinivasan@nist.gov

Compiled March 26, 2012

Low-noise, tunable wavelength-conversion through non-degenerate four-wave mixing Bragg scattering in  $\text{SiN}_x$  waveguides is experimentally demonstrated. Finite element method simulations of waveguide dispersion are used with the split-step Fourier method to predict device performance, and indicate a strong dependence of the conversion efficiency on phase matching, which is controlled by the waveguide geometry. Two 1550 nm wavelength band pulsed pumps are used to achieve tunable conversion of a 980 nm signal over a range of 5 nm with a peak conversion efficiency of  $\approx 5\%$ . The demonstrated Bragg scattering process is suitable for frequency conversion of quantum states of light. © 2012 Optical Society of America

Four-wave mixing in optical fibers has led to demonstrations of parametric amplifiers, oscillators, and wavelength convertors [1]. Recently, such processes have been observed in chip-based devices [2], where the strong modal confinement and large  $\chi^{(3)}$  in silicon and silicon nitride ( $\text{SiN}_x$ ) enhance the effective nonlinearity compared to fiber, and where group velocity dispersion (GVD) can be tailored [3] to achieve the requisite phase matching. Much of the focus is on the degenerate pump configuration, where the pump is placed near the zero GVD point of the waveguide (WG), amplifying a weak input and simultaneously generating a symmetrically-situated idler in frequency space. This has been used to show parametric gain in WGs [4] and frequency comb generation in microresonators [5, 6], but from the perspective of low-noise frequency conversion, there is a fundamental problem: signal amplification is accompanied by amplified vacuum fluctuations, which prevents operation as a noiseless quantum frequency converter [7]. Such quantum frequency conversion [8] is essential for connecting quantum systems operating at disparate wavelengths. It was recently shown on single photon states through sum-frequency generation in a few cm-long quasi-phase-matched WG [9] and four-wave-mixing Bragg scattering (FWM-BS) in a several meter long photonic crystal fiber [10]. Here, we make progress towards quantum frequency conversion in an integrated photonics platform by demonstrating FWM-BS in  $\text{SiN}_x$  WGs. We show tunable wavelength conversion of 980 nm band signals via non-degenerate telecommunications - band pumps, with a conversion efficiency reaching 5%.

In FWM-BS, two non-degenerate pump beams at frequencies  $\omega_1$  and  $\omega_2$  ( $\omega_1 > \omega_2$ ) scatter photons from a signal at  $\omega_s$  into an idler at  $\omega_i$  [11]. From conservation of energy, idlers can be produced at  $\omega_i^\pm = \omega_s \pm (\omega_1 - \omega_2)$  (Fig. 1(a)), and phase matching, effective nonlinearity, interaction length, and pump powers determine the conversion efficiency. FWM-BS directly transfers power from signal to idler, rather than from the pumps to the sig-

nal and idler. This avoids excess noise associated with parametric gain processes such as modulation interaction, which amplifies vacuum fluctuations [7]. Conversion over both small and large wavelength separations is possible if phase-matching can be obtained, and is determined by the difference in pump wavelengths.

We are interested in quantum frequency conversion of signals at  $\approx 980$  nm, for eventual use with bright, fiber-coupled InAs quantum dot (QD) single photon sources in this wavelength band [12]. Conversion will be achieved using two pump sources in the 1550 nm band (Fig. 1(a)). Choosing far red-detuned pumps with respect to the signal avoids potential stimulated Raman scattering, an important noise source in frequency converters based on fibers [13] and quasi-phase-matched WGs [9, 14]. This ensures that nearly background-free frequency conversion can be achieved. As our pump wavelength separation is limited to 30 nm, the 980 nm signal will be translated by at most  $\approx 12$  nm. Such narrowband wavelength conversion is useful for restoring spectral indistinguishability of independent QD single photon sources, for example. Broader conversion ranges are also of interest [9], and the dispersion tailoring needed is under investigation.

We calculate transverse electric polarized eigenmodes for a 550 nm tall rectangular  $\text{SiN}_x$  rib WG on a  $\text{SiO}_2$  bottom cladding (Fig. 1(b)) over a range of width  $w$  and wavelength, allowing us to estimate the dispersion relations and FWM nonlinearity. Figure 1(c) shows a plot of the dispersion parameter  $D = \frac{-2\pi c}{\lambda^2} \frac{d^2\beta}{d\omega^2}$  ( $c$  is the speed of light and  $\beta$  is the waveguide propagation constant) for  $w=800$  nm, 1000 nm, and 1200 nm WGs, indicating that as  $w$  increases, the dispersion zero redshifts and the dispersion becomes flatter. Since we are targeting conversion in the 980 nm band via telecom-wavelength pumps, we choose WG dimensions for which the dispersion zero is close to 1200 nm [11]. Conversion efficiency as a function of pump power (the pumps have equal power) is then calculated via both analytical expressions based on coupled mode theory in the

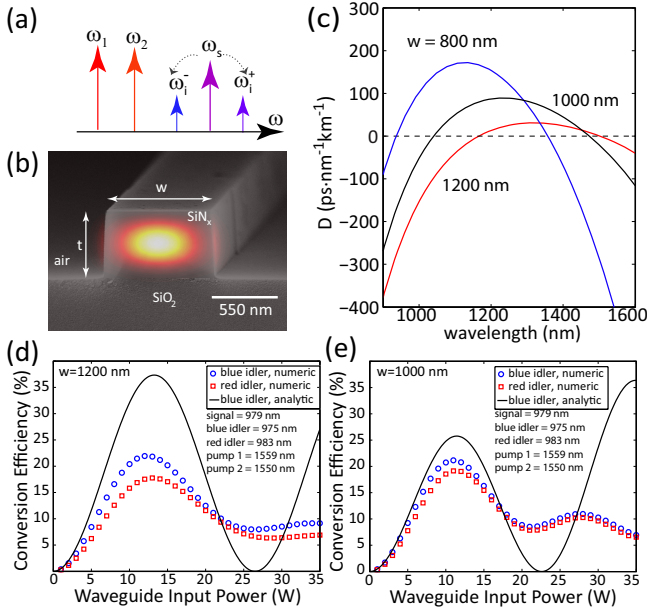


Fig. 1. (a) Schematic of FWM-BS. Pumps at  $\omega_{1,2}$  and a signal at  $\omega_s$  create blue-shifted ( $\omega_i^+$ ) and red-shifted ( $\omega_i^-$ ) idlers. (b) Fabricated  $\text{SiN}_x$  WG with superimposed fundamental TE mode profile at 1550 nm. (c) Calculated fundamental TE mode dispersion parameter  $D$  for varying  $w$ . (d)-(e) Numeric and semi-analytic results for pump power dependent conversion efficiency in 1200 nm and 1000 nm WGs. Power levels listed are for one pump; the two pumps have equal power.

non-depleted pump regime [1, 11], as well as a full-field split-step Fourier numerical simulation [1], using a WG loss of 1 dB/cm (in accordance with measurements), ellipsometric measurements of the  $\text{SiN}_x$  and  $\text{SiO}_2$  linear refractive indices, and a nonlinear refractive index  $n_2 = 2.5 \times 10^{-19} \text{ m}^2 \text{ W}^{-1}$  [15] that yields an effective nonlinearity parameter  $\gamma_{\text{eff}} \approx 6.3 \text{ W}^{-1} \text{ m}^{-1}$  for a  $w=1200$  nm WG. While the analytical solution is valid at low pump powers, it fails to account for pump depletion and undesirable effects such as multi-frequency Bragg scattering (due to secondary generated pumps). The split-step Fourier simulation alleviates this since the single field launched into the simulation includes all frequencies between the pumps and the signal/idlers, with a spectral resolution finer than the pulse bandwidth. Moreover, it takes into account higher-order dispersion (8 orders are included), and pulse-broadening and temporal walk-off effects, which can be important for short pulses and wide frequency separations. Figure 1(d)-(e) shows the results for 12 mm long WGs with  $w=1200$  nm, and  $w=1000$  nm, respectively. Both red- and blue-detuned idlers are generated (both are nearly phase-matched) with conversion efficiencies as high as 20 % predicted by the split-step calculation. Pump depletion and mixing lead to the discrepancy between the split-step and analytic results at high powers, with > 40 % of the pumps consumed by pump-pump mixing at an input power of 10 W.

We fabricate 12 mm long rib WGs (Fig. 1(b)) through electron-beam lithography and reactive ion etching of a 550 nm thick  $\text{SiN}_x$  layer grown on top of a 3  $\mu\text{m}$   $\text{SiO}_2$  layer, all on a Si substrate [6]. The experimental setup is shown in Fig. 2(a). To measure WG conversion bandwidth, two amplified 1550 nm band continuous wave (cw) pumps are combined with a weak signal at 977.4 nm and sent into 1000 nm and 1200 nm wide WGs via a lensed optical fiber. Light is collected at the WG output with a lensed fiber and routed to a wavelength division multiplexer (WDM) that separates the pumps from the signal and idlers. The pumps are monitored on an optical spectrum analyzer (OSA), while a grating spectrometer with a silicon CCD measures the generated idlers and residual signal light, which is suppressed by 53 dB using a fiber Bragg grating (FBG) placed before the spectrometer input. Pump 1 is swept between 1535 nm and 1565 nm, while pump 2 is fixed at 1565 nm. Both FWM-BS generated  $w_i^\pm$  idlers are visible around the signal, and move symmetrically away from it as the separation between the pumps increases (Fig. 2(b)), in agreement with energy conservation. The conversion bandwidth can be deduced from Fig. 2(c), where the conversion efficiency  $P_i/P_s$  for both idlers is plotted ( $P_i, P_s$  are the idler and signal powers at the WG output). The 1200 nm WG has a broader conversion bandwidth than the 1000 nm WG.

To achieve the high peak powers needed for more efficient conversion, pulses from a 80 MHz repetition-rate mode-locked laser are filtered by 1 nm wide bandpass filters at 1550 nm and 1559 nm, respectively. The pulses, with a measured full-width at half-maximum of  $4.2 \text{ ps} \pm 1 \text{ ps}$ , are each amplified by a 1 W erbium-doped fiber amplifier (EDFA) and temporally overlapped by a tunable optical-delay line before being combined with a weak 979 nm cw signal and sent into the WG. To determine peak power while avoiding spurious effects in the OSA, the average power is first measured at low amplification and scaled by the duty cycle. An auxiliary  $\text{SiN}_x$  WG showing efficient 3rd harmonic generation is used to calibrate peak powers at higher amplification, as the 3rd harmonic signal scales with the cube of the peak power. This allows us to estimate a maximum peak power inside the WG of  $\approx 6.8 \text{ W}$  (accounting for  $\approx 6 \text{ dB}$  coupling loss per facet). Keeping the pump and signal wavelengths at 1559 nm, 1550 nm, and 979 nm, respectively, the coupled power is varied between 0.5 W and 6.8 W, and the converted idlers are measured at the WG output. The conversion efficiency, which takes into account that the input signal is cw while the pumps are pulsed, is determined by integrating over the idler spectrum, scaling by the pulse duty cycle, and dividing by the integrated signal power.

Figure 3(a) shows measured conversion efficiency for the blue-shifted idler as a function of peak input power. The data follows the calculated trend and reaches a maximum of  $\approx 2.5 \%$ . When the longer wavelength pump is moved to 1557 nm, where the laser power is higher and phase-mismatch is reduced, the overall conversion efficiency increases to  $\approx 5 \%$  (inset to Fig. 3(a)). Higher

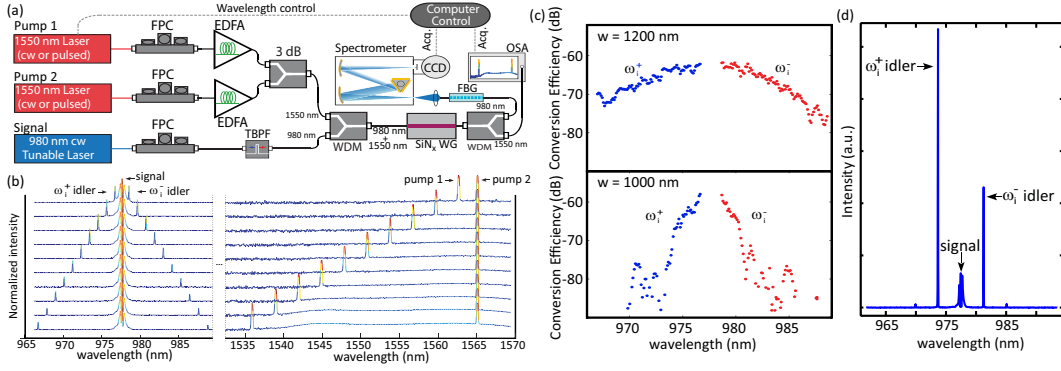


Fig. 2. (a) Experimental setup. FPC=fiber polarization controller. (b) Simultaneous spectrometer (980 nm band) and OSA (1550 nm band) acquired spectra of residual signal, generated idlers, and pumps 1 and 2, for varying pump 1 wavelengths. (c) Conversion efficiencies for  $\omega_i^\pm$  idlers as functions of idler wavelength for  $w = 1200$  nm and  $w = 1000$  nm WGs. (d)  $w = 1000$  nm WG output spectrum under pulsed (1 ns width) pumping with 6.5 W peak pump power. The residual signal is suppressed relative to (b) due to use of a second FBG rejection filter.

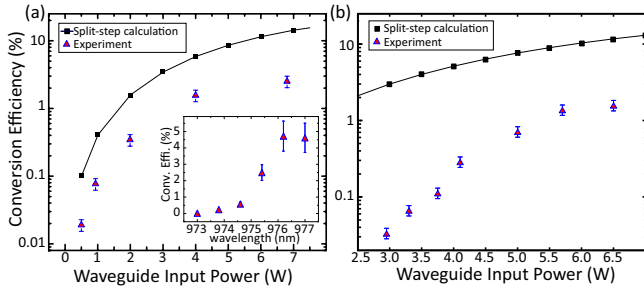


Fig. 3. (a) Conversion efficiency vs. peak pump power for a 975 nm idler (signal at 979 nm) in a  $w = 1200$  nm WG, using ps pump pulses. Inset shows the conversion efficiency for different blue-shifted idler wavelengths. (b) Conversion efficiency vs. peak pump power in a  $w = 1000$  nm WG, using ns pump pulses. Error bars are due to uncertainty in the measurement of pulse pump width, and represent one standard deviation. Power levels listed are for one pump; the two pumps have equal power.

conversion levels may be possible by increasing the pump power by a factor of 2 (Fig. 1(d)), using longer WGs, and more precise dispersion tailoring. In particular, we note that the measured conversion efficiency is consistently lower than predicted. While imprecise knowledge of input power into the WG and the effective nonlinearity plays a role in this discrepancy, split-step simulations indicate that non-optimal dispersion can be a dominant factor. Small changes in the WG thickness ( $\approx 25$  nm, occurring due to fluctuations in the  $\text{SiN}_x$  growth rate) are predicted to cause significant changes in the conversion efficiency, with a stretching and shifting of the conversion efficiency peaks in Fig. 1(a) to higher powers.

We next studied conversion in the 1000 nm width WG. In addition to a different WG and resulting dispersion profile, we also used 1 ns long pulses with similar peak-powers to the earlier implementation, by intensity modulating 1559 nm and 1550 nm cw lasers with a sin-

gle electro-optic modulator and amplifying the resultant pulses in an EDFA. This allowed us to study device behavior in the nanosecond regime, of particular importance for wavelength conversion of single photons from quantum dots, whose characteristic timescale is on the order of 1 ns. Figure 3(b) shows the conversion efficiency as a function of pump power for a range of input powers, reaching a maximum of 1.3 %, which is around half the efficiency of the 1200 nm WG at the same peak power. The loss of conversion and deviation from the predicted trend at lower powers is most likely due to the degradation of the WGs during the course of data accumulation (data was recorded from high to low power), resulting from the high pulse energies. Importantly, despite these high energies, no excess noise is measured in the conversion bands (Fig. 2(d)), suggesting that if the efficiency can be improved, background-free quantum frequency conversion can be achieved in these devices.

In conclusion, we have demonstrated chip-scale wavelength conversion in a silicon nitride waveguide through the process of four-wave mixing Bragg scattering. The background-free nature of this approach should enable frequency conversion of quantum states of light. This work complements recent demonstrations of single photon generation [16], entanglement manipulation [17], and detection [18] in a silicon platform in the effort to develop integrated quantum photonic circuits on a chip.

We thank Houxun Miao and Rich Kasica for help with fabrication, Nanh Van Nguyen for ellipsometric measurements, and the DARPA MESO program for partial support. I.A and M.D. acknowledge support under the Cooperative Research Agreement between the University of Maryland and NIST-CNST, Award 70NANB10H193.

## References

1. G. P. Agrawal, *Nonlinear Fiber Optics* (Academic Press, Amsterdam, 2007).
2. Q. Lin, O. J. Painter, and G. P. Agrawal, "Nonlinear optical phenomena in silicon waveguides: modeling and

- applications,” *Optics Express* **15**, 16 604 (2007).
3. A. C. Turner, C. Manolatou, B. S. Schmidt, M. Lipson, M. A. Foster, J. E. Sharping, and A. L. Gaeta, “Tailored anomalous group-velocity dispersion in silicon channel waveguides,” *Optics Express* **14**, 4357–4362 (2006).
  4. M. A. Foster, A. C. Turner, J. E. Sharping, B. S. Schmidt, M. Lipson, and A. L. Gaeta, “Broad-band optical parametric gain on a silicon photonic chip,” *Nature* **441**, 960–963 (2006).
  5. J. S. Levy, A. Gondarenko, M. A. Foster, A. C. Turner-Foster, A. L. Gaeta, and M. Lipson, “CMOS-compatible multiple-wavelength oscillator for on-chip optical interconnects,” *Nature Photonics* **4**, 37–40 (2010).
  6. F. Ferdous, H. Miao, D. E. Leaird, K. Srinivasan, J. Wang, L. Chen, L. T. Varghese, and A. M. Weiner, “Spectral line-by-line pulse shaping of on-chip microresonator frequency combs,” *Nature Photonics* **5**, 770–776 (2011).
  7. C. McKinstrie, J. Harvey, S. Radic, and M. Raymer, “Translation of quantum states by four-wave mixing in fibers,” *Opt. Express* **13**, 9131–9142 (2005).
  8. P. Kumar, “Quantum Frequency-Conversion,” *Opt. Lett.* **15**, 1476–1478 (1990).
  9. M. T. Rakher, L. Ma, O. Slattery, X. Tang, and K. Srinivasan, “Quantum transduction of telecommunications-band single photons from a quantum dot by frequency upconversion,” *Nature Photonics* **4**, 786–791 (2010).
  10. H. J. McGuinness, M. G. Raymer, C. J. McKinstrie, and S. Radic, “Quantum Frequency Translation of Single-Photon States in a Photonic Crystal Fiber,” *Phys. Rev. Lett.* **105**, 093 604 (2010).
  11. K. Uesaka, K. Kin-Yip, M. Marhic, and L. Kazovsky, “Wavelength exchange in a highly nonlinear dispersion-shifted fiber: Theory and experiments,” *IEEE J. Sel. Top. Quan. Elec.* **8**, 560–568 (2002).
  12. M. Davanço, M. T. Rakher, , W. Wegscheider, D. Schuh, A. Badolato, and K. Srinivasan, “Efficient quantum dot single photon extraction into an optical fiber using a nanophotonic directional coupler,” *Appl. Phys. Lett.* **99**, 121 101 (2011).
  13. A. H. Gnauck, R. M. Jopson, C. J. McKinstrie, J. C. Centanni, and S. Radic, “Demonstration of low-noise frequency conversion by Bragg scattering in a fiber,” *Opt. Express* **14**, 8989–8994 (2006).
  14. C. Langrock, E. Diamanti, R. Roussev, Y. Yamamoto, M. Fejer, and H. Takesue, “Highly efficient single-photon detection at communication wavelengths by use of upconversion in reverse-proton-exchanged periodically poled LiNbO<sub>3</sub> waveguides,” *Opt. Lett.* **30**, 1725–1727 (2005).
  15. D. T. H. Tan, K. Ikeda, P. C. Sun, and Y. Fainman, “Group velocity dispersion and self phase modulation in silicon nitride waveguides,” *Appl. Phys. Lett.* **96**, 061 101 (2010).
  16. M. Davanço, J. R. Ong, A. B. Shehata, A. Tosi, I. Agha, S. Assefa, F. Xia, W. Green, S. Mookherjee, and K. Srinivasan, “Telecommunications-band heralded single photons from a silicon nanophotonic chip,” *ArXiv:1201.2659* (2012).
  17. D. Bonneau, E. Engin, K. Ohira, N. Suzuki, H. Yoshida, N. Iizuka, M. Esaki, C. Natarajan, M. Tanner, R. Hadfield, S. Dorenbos, V. Zwiller, J. O’Brien, and M. Thompson, “Quantum interference in silicon waveguide circuits,” in *8th IEEE International Conference on Group IV Photonics (GFP)* pp. 1–3 (2011).
  18. W. Pernice, C. Schuck, O. Minaeva, M. Li, G. Goltsman, A. Sergienko, and H. Tang, “High Speed Travelling Wave Single-Photon Detectors with Near-Unity Detection Efficiency,” *ArXiv:1108.5299* (2011).